LAWRENCE
LIVERMORE
NATIONAL
LABORATORY

LLNL-JRNL-643808

The Reactivity of Energetic Materials Under High Pressure and Temperature

M. R. Manaa, L. E. Fried

September 17, 2013

Advances in Quantum Chemistry

Disclaimer

The Reactivity of Energetic Materials under high Pressure and Temperature

M. Riad Manaa and Laurence E. Fried
Lawrence Livermore National Laboratory
Energetic Materials Center

In the brief instant of a high-explosive detonation, the shock wave produces a pressure 500,000 times that of the Earth's atmosphere and internal temperatures soar up to 5,500 Kelvin. The detonation wave travels as fast as 10 kilometers per second. As the shock propagates through the explosive, the rapid heating coupled with compression that results in an almost 30% volume reduction, initiates complex chemical reactions. A dense, highly reactive supercritical fluid is established behind the propagating detonation front. The energy release from the exothermic chemical reactions drive and sustain the detonation process until complete reactivity is achieved. Several experimental results suggest the existence of strong correlations between the applied mechanical stress and shocks, the local heterogeneity and defects (dislocations, vacancies, cracks, impurities, etc.), and the onset of chemical reactions. [1-6] The reaction chemistry of energetic materials at high pressure and temperature is, therefore, of considerable importance in understanding processes that these materials experience under impact and detonation conditions. Chemical decomposition models are critical ingredients in order to predict, for example, the measured times to explosion and the conditions for ignition of hot spots, [7] the localized regions of highly concentrated energy associated with defects. [8,9] From a more applied prospective, understanding reaction mechanisms has important ramifications in decomposing such materials safely and cheaply, as there exist vast stockpiles of high explosive materials with corresponding environmental hazards related to earth and groundwater contamination. [10]

Detailed investigation of the kinetics and decomposition mechanisms and general reactivity in explosive materials is critical in order to improve the accuracy and reliability of micromechanical models that are implemented in computational continuum codes. The

time frame associated with explosive reactions and the highly exothermic conditions associated with an explosion make experimental investigation of the decomposition pathways difficult at best. Elucidating decomposition pathways is further complication due to the increased instability of explosive materials under high temperature and pressure regimes. At present, computer simulations at the atomistic level provide the best access to the short time scale processes (~100 femtoseconds (fs) to a few tens of ps) occurring in regions of extreme conditions. Computational investigations aspire to unravel at the molecular level the detailed decomposition pathways and the kinetic rate laws at high-pressure and temperature. The ultimate objective of such studies is to construct accurate and predictive models of performance and sensitivity for the development of new energetic materials. [11,12]

Below, we briefly discuss methods used to simulate the chemistry of shocked energetic materials, with some emphasis on methods employed in our studies. We next examine the chemical reactivity of the two explosives HMX and TATB from condensed-phase atomistic simulations using the quantum-based method density-functional tight-binding[13].

METHODS TO SIMULATE CHEMISTRY AT EXTREME CONDITIONS

The chemical reactions of energetic materials at extreme conditions present significant challenges to simulation methodologies. Energetic materials release energy through complex multi-step pathways. The measured reaction time of a detonating high explosive, called the "reaction zone length" is inferred from hydrodynamic measurements to be on the ns-μs timescale, depending on the material under study. These times are

exceedingly long when compared to a typical molecular dynamics time step (0.5 fs).

High explosives are compressed by the shock wave before they react, with a typical pressure before reaction of 40 GPa (400 kbar). These pressures are sufficient to fundamentally change the nature of chemical bonding. As matter is compressed, the mean electron kinetic energy increases. The increase in kinetic energy leads to weakening of chemical bonds, and an increase in ionization.[14] The extreme environment of a detonation demands that chemistry be modeled in the condensed phase. Condensed phase electronic structure approaches based on Kohn-Sham density functional theory[15] are typically used to simulate systems of up to several hundred atoms for times on the order of 10 ps.[16-20] A system of several hundred atoms could be represent only 10 energetic molecules (for example, TATB has 24 atoms). Therefore, standard DFT approaches are very limited both in terms of system size and simulation duration when applied to condensed phase energetic molecular chemistry.

One approach to extend both time and spatial scales is to employ reactive empirical force fields to represent intermolecular interactions. The ReaxFF force field[21] has been used to study the chemistry of a number of energetic materials. The ReaxFF approach is scalable for systems with thousands of atoms, and time scales roughly up to a ns. ReaxFF has been used to study thermal and shock decomposition processes of various energetic systems [22-28]. One of the difficulties of the ReaxFF approach, however, are the many parameters used in the force field. The determination of optimal parameters is not unique, and parameters are typically refined for particular applications[25] . The ReaxFF method scales almost linearly with the number of atoms[29], and therefore is potentially applicable to very large system sizes. The wide variety of chemical environments

encountered during the complex chemistry of HE decomposition could be difficult to represent adequately with a force field approach.

A second approach is to employ more approximate forms of quantum simulation that could enable longer simulation times and larger system sizes. Unlike reactive force fields, quantum based methods permit us for the first time to examine electronic properties at detonation conditions. Semi-empirical, quantum based methods such as tight binding are less costly, extending the time profile of chemical events to be investigated for a few hundred ps of computational cells of several hundred atoms. Recent studies with variants of tight-binding methods include shocked benzene, [30] shocked methane, [31,32], the chemistry of dense HMX explosive, [33,34], shocked nitromethane, [35], shocked and dense TATB explosive, [36], and complete reactivity of detonating HN_3. [37]

Our group has applied the Density Functional Tight Binding with self-consistent charges (DFTB) approach to high explosive reaction chemistry[19,35] . DFTB is an approximate quantum method that uses a minimal basis set to represent covalent interactions. Unlike DFT, DFTB contains an empirical repulsive force field that is fit to experimental data and DFT simulations. The two body DFTB repulsive force field, however, is much simpler in form than the many-body interactions represented in ReaxFF. A DFTB calculation is 10-100 times faster than a DFT calculation. Since the DFTB method requires a matrix diagonalization, the technique has an N^3 asymptotic scaling with the number of atoms. Linear scaling methods can be adapted to DFTB, but most implementations to date have not done so. In practice, this limits the system size of a DFTB molecular dynamics simulation to several hundred atoms. The increased

efficiency of DFTB has allowed simulations to be conducted for as long as 2 ns.

Since DFTB the method is semi-empirical, its accuracy for energetic materials should be verified through comparison to experiment and other simulations. DFTB has been benchmarked against DFT for the static compression of nitromethane[38] and the reactivity of nitromethane[19]. These comparisons showed that qualitatively similar results were obtained with DFT Generalized Gradient Approximation[39] (GGA) and DFTB. In benchmarking against the reaction energy of small organic molecules, DFTB was found to have a mean absolute error of 12.5 kcal/mol when compared to experiment. Although the DFTB method is not as accurate as more elaborate ab initio methods, the high temperature condition of the simulation ameliorates this difficulty. For instance, at 3500K a 10 kcal/mol error in a reaction barrier leads to a factor of 4 error in the reaction rate. This is an acceptable error for a qualitative study. At 600K, however, a comparable error in the barrier would lead to a factor of 4000 in the reaction rate.

Recent work has been undertaken to improve the accuracy of DFTB by adding higher-order corrections to charge fluctuations[40], extending the repulsive energy terms[41,42], and by using non-minimal basis sets[42]. Goldman et al. showed that DFTB simulations with a non-minimal basis could be successfully applied to shocked carbon at pressures in excess of 10 Mbar, while the standard DFTB implementation showed significant errors when compared to experiment. In Figure 1 we show a comparison of the improved DFTB method of Goldman et al.[42] to DFT GGA calculations. The DFT GGA calculations are in good agreement with experiment (not shown), although the spread of results from different experimental studies is large.

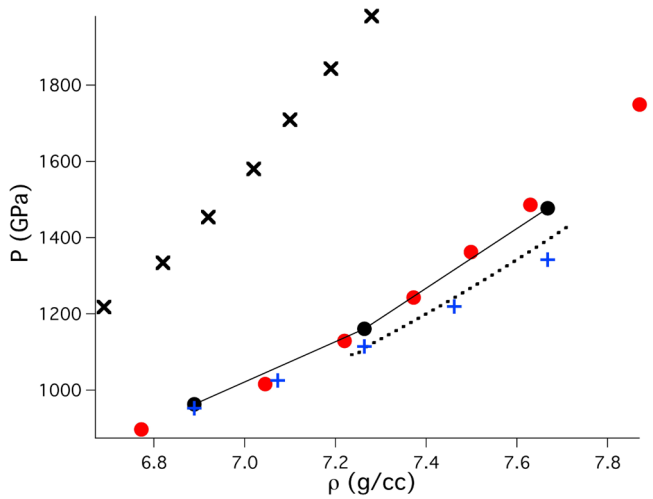

Figure 1: Comparison of simulation and experimental results for the pressure and density of shocked carbon. The black "x" symbols are standard DFTB. The filled red symbols are DFTB including a polarized basis set. The closed black and blue "+" symbols are GGA DFT calculations.

Energetic material detonation involves the propagation of a supersonic shock wave. Therefore, the study of the chemistry of detonation requires that some sort of approximation to the shock be made. One of the simplest approximations is to simply study the system at a fixed density and temperature. While this is a well defined statistical mechanics problem, it does not correspond closely to an actual shock wave. The exothermic nature of energetic material reactivity necessarily leads to a large change in the temperature upon reaction. This change is suppressed when the temperature is fixed in a molecular dynamics simulation. Simulations at fixed volume and energy do not have this difficulty, but still miss important features of the shock wave.

The shock wave itself is a traveling mechanical excitation in the material, with a typical velocity of 8 km/s. When converted into typical molecular dynamics units, this is

8 nm/ps. Therefore, the wave propagating through the material will move 800 nm in a 100 ps simulation. This is much larger than most the system size in most reactive molecular dynamics simulations, especially those using quantum methods (a simulation cell size of 5-10 nm is typical). There are several approaches to overcome this problem. One approach is to employ direct numerical simulations for shorter timescales of several ps[43]. Another is to use a moving frame of reference of some sort in simulating the shock wave.

Reed et al.[44] developed a method with a moving frame of reference called the multiscale shock simulation technique (MSST). MSST allows both the system density and temperature to vary in a way that conserves mass, momentum, and energy during the shock wave evolution. It has been known since the 1940's that high explosives expand and move toward lower pressure states as they react in the shock front. The macroscopic theory describing this is called the Zeldovich-von Neumann-Doering (ZND) theory[45]. The MSST can be thought of as coupling the macroscopic ZND theory to the MD simulation cell. There are alternative approaches to implementing molecular dynamics in a moving frame. One such technique is to inject particles on one side of the simulation cell, and remove particles on the other side. A second approach is to employ a fixed density but constrain the temperature according to macroscopic hydrodynamics, which is implemented in the Hugoniotstat technique by Maillet et al[46].

The MSST has been successfully compared to both continuum direct numerical simulations and to molecular dynamics direct numerical simulations. In Figure 2 we show a comparison between the MSST and direct numerical simulation for a shock wave in amorphous solid carbon. Nonetheless, it is important to remember that the MSST does

not treat density gradients, and therefore is less accurate very near the shock front where density gradients are very high. Recently the MSST has been extended to include electronic excitations[47].

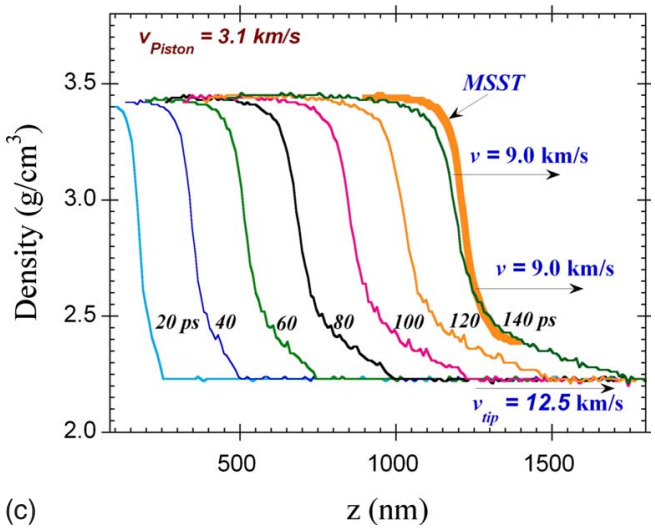

Figure 2: Comparison of a shock wave profiles in amorphous carbon (thin solid lines) with a velocity of 9.0 km/s compared to the MSST method (thick gold line), also at a velocity of 9.0 km/s. The MSST method does not include the non-steady foot in the shock wave profile, which propagates at the velocity v_{tip}.

It is known that the shock initiation of energetic materials is sensitive to micron-scale material structure, such as the presents of voids, particle size, and plastic bonded binder. It is difficult to treat these phenomena at the atomic scale. Instead, we have focused on overdriven shock waves that propagate at velocities greater than that of a steady detonation, or on simulations under a fixed temperature above 2000K. Under these conditions, the HE transforms in a ps or less to a highly reactive dense fluid phase. There are important differences between the dense fluid (supercritical) phase and the

solid phase, which is stable at standard conditions. Namely, the dense fluid phase cannot accommodate long-lived voids, bubbles, or other static defects. Instead numerous fluctuations in the local environment occur within a timescale of 10s of fs. The fast reactivity of the dense fluid phase and the short spatial coherence length make it well suited for molecular dynamics study with a finite system for a limited period of time, although it should be remembered that overdriven shock waves do not correspond to the most commonly performed experiments for energetic materials.

The quantum nature of molecular vibrations poses an additional challenge to simulations of reactive chemistry at extreme conditions. Molecular dynamics simulations predict a classical heat capacity regardless of whether the force field is empirical or calculated via quantum simulations. The classical heat capacity can be significantly greater than the quantum (experimental) heat capacity for materials that are rich in hydrogen. Goldman et al. have developed a method to correct shock temperatures obtained through MD simulations for quantum vibrational effects. In Figure 3 we show a comparison of simulated and experimental temperatures for shocked methane. Although methane is not an energetic material, it is an expected detonation product. One potential route to developing insight into the chemistry of shocked energetic materials is to study the simpler problem of detonation product mixtures[48].

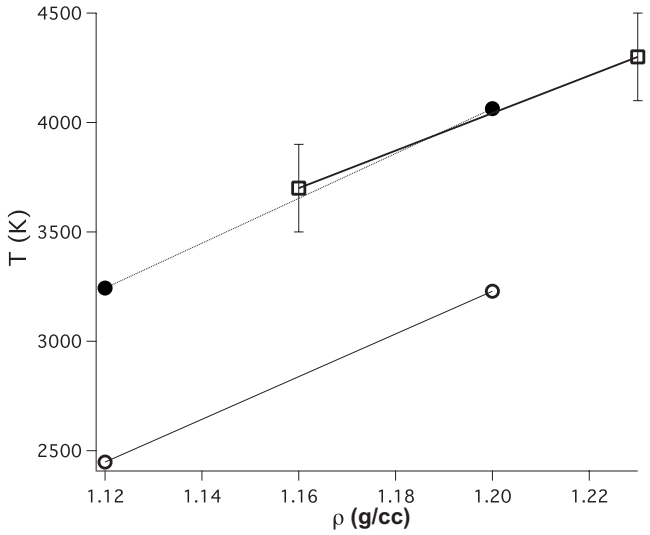

Figure 3: Plot of the temperature vs. density for shocked CH_4. The open circles correspond to the classical ionic temperatures from a DFT calculation, the solid circles are values corrected for quantum effects as in Goldman et al.[49] The open squares with error bars show experimental results.

Recently the MSST has been modified to include a vibrational quantum correction through the use of a colored noise Langevin thermostat[32].

We mention a final difficulty in simulations of chemistry at extreme conditions, which is the chemical interpretation of results. Under the high temperature and pressure conditions of a detonation, reaction rates are predicted by simulations to be comparable to inverse vibrational periods. This makes it difficult to unambiguously determine molecular species and chemical reactions at extreme conditions. The physical basis of this issue is that as matter is compressed, it becomes increasingly non-molecular. A good example of this phenomenon is found in water, where increasing compression has been shown to lead to hydrogen bond symmetrization and non-molecular phases. In simulations of PETN at high density and temperature, Wu et al.[50] found that hydrogen

diffused at a much higher rate than other atoms. An example is shown in Figure 4, where we show the motion of hydrogen and other elements in "unwrapped" coordinates.

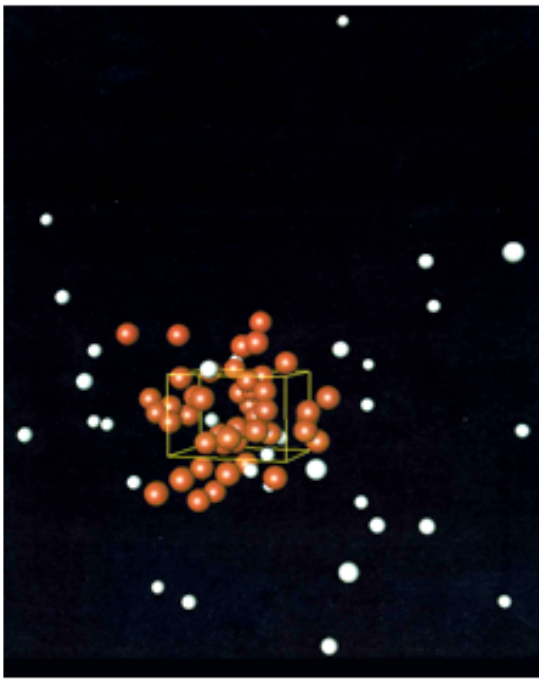

Figure 4: The simulated positions of hydrogen atoms (white) and other elements (C,N,O) (orange) are shown relative to the initial simulation cell (yellow box). The hydrogen atom diffuse much further than the other elements, indicating that hydrogen has taken on a non-molecular character.

We identify molecular species in our simulations as follows: a bond distance and bond duration are both used to determine whether two molecules are bonded. This approach is independent of the method used to calculate forces. For instance, reactive force fields often have a distance-dependent bond order parameter. Bond order parameters, however, are more difficult to generate in quantum simulations. We determine the bond distance by identifying the first minimum in the atom-atom radial distribution function[51]. This corresponds to the maximum of the potential of mean force,

which is a nature effective interaction potential in a many-body condensed phase environment. We next determine the bond duration to be equal to a several times a typical vibrational period. This enforces a loose timescale separations between molecules and vibrations. We find that using these criteria leads to reasonable (though not unique) identifications of molecular species in complex reactive environments.

CHEMISTRY OF HMX

HMX (1,3,5, 7-tetranitro-1, 3,5,7-tetraazacyclooctane, figure 5) is widely used as an ingredient in various explosives and propellants. A molecular solid at standard state, it has four known polymorphs. We have conducted a quantum-based molecular dynamics simulation of the chemistry of HMX under extreme conditions, similar to those encountered at the Chapman-Jouget detonation state. [34] The simulation studied the reactivity of dense (1.9 g/cm^3) fluid HMX at 3500K for reaction times of up to 55 ps, thus allowing the formation of stable product molecules. There are numerous experimental characterizations at low temperatures (i.e. < 1000 K, well below detonation temperature) of decomposition products of condensed-phase HMX. [52-64] These studies tend to identify final gas products (such as H_2O, N_2, H_2, CO, CO_2, etc.) from the surface reactions and aspire to establish a global decomposition mechanism. The early thermal decomposition study using mass spectrometry at T=503, 527, and 553 K of Syryanarayana et al. [62] identified a concerted decomposition into four methylenenitramine ($CH_2N_2O_2$), which can further decompose into CH_2O and N_2O. At 448-548 K, Farber and Srivastava [58] identified a major decomposition product with m/e=148 and proposed a homolytic cleavage of HMX to two $C_2H_4N_4O_4$ fragments. CH_2N and NO_2 were later detected as later stage decomposition products from an $CH_2N_2O_2$

intermediate in an electron spin resonance pyrolysis study. [60] Experiments using thermogravimetric modulated beam mass spectrometry and isotope scrambling identified gaseous pyrolysis products such as H_2O, HCN, CO, CH_2O, NO, and N_2O between 483 and 508 K. [52-54] Brill et al. have analyzed rate measurements for the early stage of HMX thermal decomposition, [56] revealing the existence of an approximate linear relationship between the Arrhenius prefactor, ln A, and the apparent activation energy, E_a. Brill later suggested two competing global mechanisms for thermal decomposition, the first leading to 4 HONO and 4 HCN, while the second leads to the formation of 4 CH_2O and 4 N_2O. [55]

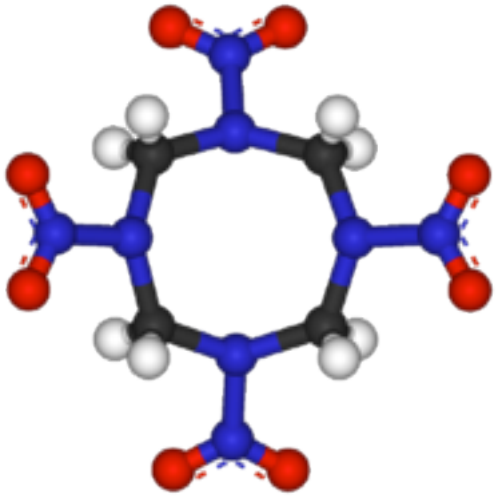

Figure 5. Molecular HMX.

The above experimental work on the thermal decomposition of condensed phase HMX is largely restricted to relatively low temperature (~550 K) and pressure (0.1 GPa) regimes. Similar experimental observations at detonation conditions (temperatures 2000-5000 K, and pressure 10-30 GPa), however, have not been realized to date. At present, computer simulations provide the best access to the short time scale processes occurring

in these regions of extreme conditions of pressure and temperature. [65] Many computational studies have included electronic structure calculations of various decomposition channels of the gas-phase HMX molecule. For example, Melius determined decomposition pathways for nitramine compounds HMX and RDX at the MP4 level of theory. He found that the initial step in decomposition is N-NO_2 bond breaking, which subsequently causes a significant weakness in the second-nearest-neighbor bond breaking energies (18 kcal/mol for the C-N bond dissociation), leading to HCN, NO_2, and H as the net products for rapid thermal heating. In the condensed phase, however, Melius made the observation that alternative decomposition mechanisms can occur. The free NO_2 fragment can recombine as a nitride, which then decomposes to form NO, or attract weakly bound hydrogen atoms and form HONO. The HONO molecules can then rapidly equilibrate to form water via the reaction $2HONO \rightarrow H_2O + NO_2 + NO$. [66]

Lewis et al. calculated four possible decomposition pathways of the α-HMX polymorph: N-NO_2 bond dissociation, HONO elimination, C-N bond scission, and the concerted ring fission. Based on the energetics, it was determined that N-NO_2 dissociation was the initial mechanism of decomposition in the gas phase, while they proposed HONO elimination and C-N bond scission to be favorable in the condensed phase. [67] The more recent study of Chakraborty et al., using the DFT (B3LYP) method, reported detailed decomposition pathways of β-HMX, the stable polymorph at room temperature. It was concluded that consecutive HONO elimination (4 HONO) and subsequent decomposition into HCN, OH and NO are energetically the most favorable pathways in the gas phase[68]. Zhang et al. have concluded from their ReaxFF study that

only small gas fragments occur during the thermal decomposition of HMX, in contrast to the formation of large clusters obtained from decomposing TATB. [69] To date, however, our study remains the only quantum-based study of the fast chemistry of condensed-phase HMX at conditions similar to those encountered under detonation.

In our molecular dynamics simulations, we used DFTB to calculate the forces on atoms.[13] The initial condition of the simulation included six HMX molecules in a cell, corresponding to the unit cell of the δ phase of HMX, with a total of 168 atoms. It is well known that HMX undergoes a phase transition at 436 K from the β phase (two molecules per unit cell with a chair molecular conformation, density = 1.89 g/cm^3) to the δ phase (with boat molecular conformation, density=1.50 g/cm^3). [70] The δ phase was chosen as the initial starting structure to include all the relevant physical attributes of the system prior to chemical decomposition. The calculation started with the experimental unit cell parameters and atomic positions of δ HMX. The atomic positions were optimized in an energy minimization procedure.

The cell was then compressed to the final density of the simulation. The atomic structure was subsequently fully optimized at the corresponding cell volume. Since the purpose of the simulation is to study the high- pressure and high- temperature chemistry of HMX in general, the exact density and temperature used in our simulation is somewhat arbitrary. The density of 1.9 g/cm^3 and a temperature of 3500 K were chosen. This state is in the neighborhood of the Chapman-Jouget state of β-HMX (3500 K, 2.1 g/cm^3) as predicted through thermochemical calculations described later. The closest experimental condition corresponding to this simulation would be a sample of HMX, which is suddenly heated under constant volume conditions, such as in a diamond anvil cell.

The molecular dynamics simulation was conducted at constant volume and constant temperature. Periodic boundary conditions were imposed. Constant temperature conditions were implemented through velocity rescaling. A time-step of 0.5 fs was used.

Under the simulation conditions chemical reactions occurred within 50 fs. Stable molecular species were formed in less than one ps. Figs. 2 (a-d) display the product formation of H_2O, N_2, CO_2 and CO, respectively. The concentration, C (*t*), is represented by the actual number of product molecules formed at the corresponding time *t*. Each point on the graphs (open circles) represents a 250 fs averaged interval. The number of the molecules in the simulation was sufficient to capture clear trends in the chemical composition of the species studied. These concentrations were in turn fit to an expression of the form: $C(t) = C_\infty (1 - e^{-bt})$, where C_∞ is the equilibrium concentration and b is the effective rate constant. From this fit to the data, we estimate effective reaction rates for the formation of H_2O, N_2, CO_2, and CO to be 0.48, 0.08, 0.05, and 0.11 ps^{-1}, respectively.

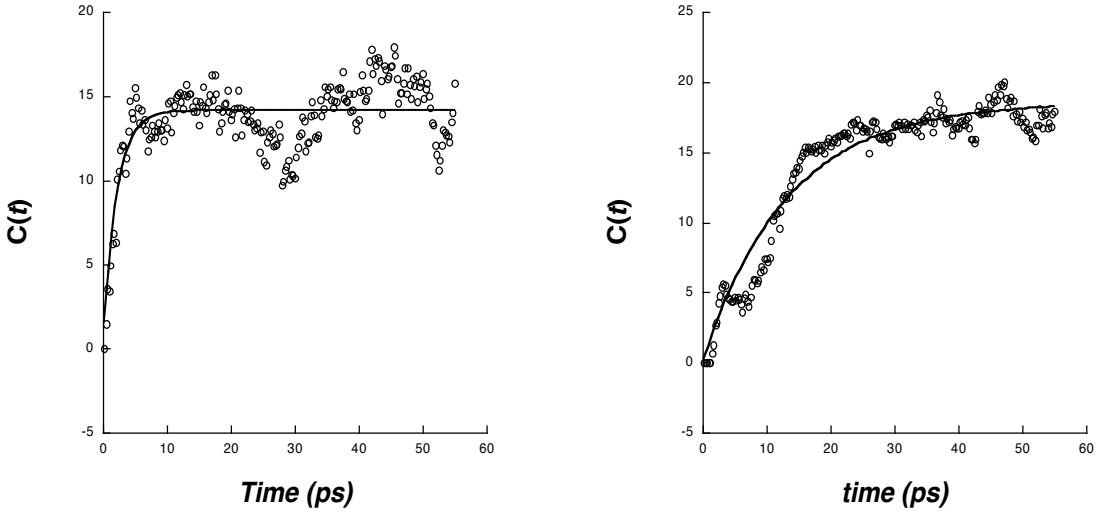

a

b

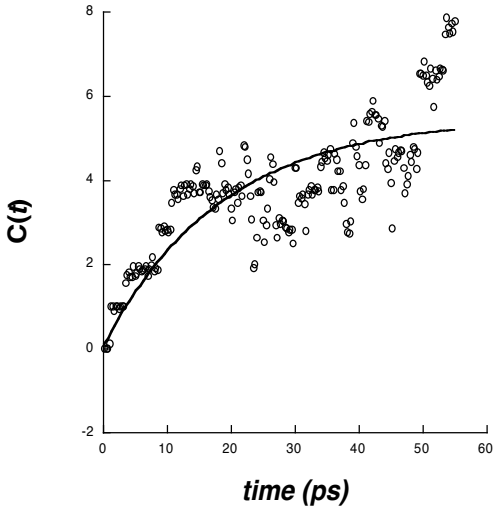

c

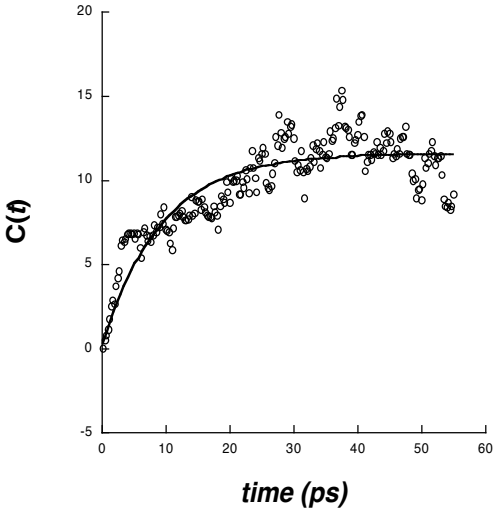

d

Figure 6. Product particle-number as a function of time for (a) H_2O, (b) N_2, (c) CO_2, and (d) CO.

It is not surprising that the rate of H_2O formation is much faster than that of N_2. Fewer reaction steps are required to produce a triatomic species like water, while the formation of N_2 involves a much more complicated mechanism. [66] The formation of water (Fig.2-a) starts around 0.5 ps and reaches a steady state at 10 ps, with oscillatory behavior of decomposition and formation clearly visible. The formation of N_2 (Fig.2-b), on the other hand, starts around 1.5 ps and is still progressing (slope of the graph is slightly positive) after 55 ps of simulation time.

In Fig.3 we show a comparison of dominant species formation for decomposing HMX obtained from an entirely different theoretical approach. The concentration of species at chemical equilibrium were calculated through thermodynamic calculations, as implemented within the Cheetah thermochemical code. [71,72] For HMX, the molecules N_2, H_2O, CO_2, HNCO, and CO were predicted to be present in quantities greater than 1 mol/kg HMX. The species CO, NH_3, H_2, CH_4, H, CH_3OH, NO, and C_2H_4 were also predicted to be present in quantities greater than 0.0001 mol/kg HMX. The species N_2O, C_2H_2, N, O, O_2, NO_2, HCN, atomic C, and O_3 were not predicted to have significant concentrations. Carbon in the diamond phase was predicted to be in equilibrium with the other species at a concentration of 4.9 mol/kg HMX. The thermochemical calculations predict a pressure for fully reacted HMX of 16 GPa, or 160 kBar.

As can be noticed in Fig.3, the results of the MD simulation compare very well with the formation of H_2O, N_2, and HNCO. The relative concentration of CO and CO_2, however, is reversed at the end of the simulation. This could be due to the limited simulation time. No condensed carbon was found in the current simulation.

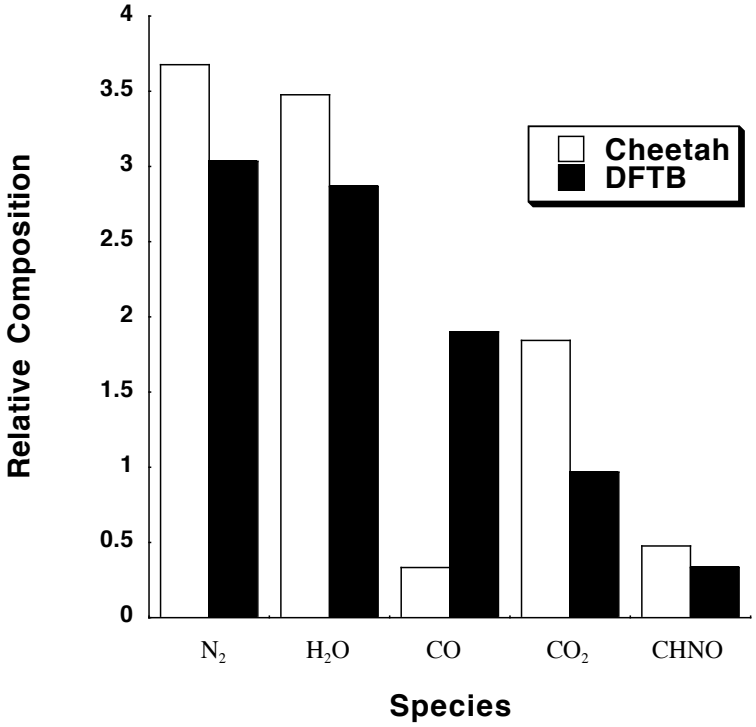

Figure 7. Comparison of relative composition of dominant species determined from current DFTB simulation and from a thermodynamical calculation.

One expects more CO_2 than CO as final products, as predicted by Cheetah (Fig.3). The results displayed in Figs.2 (c-d) show that, at simulation time of 40 ps, the system is still in the second stage of reaction chemistry. At this stage, the CO concentration is rising and has not yet undergone the water gas shift reaction ($CO + H_2O \rightarrow CO_2 + H_2$) conversion. Interestingly, this shift seems to occur at around 50 ps of the simulation, with CO_2 molecules being formed while CO concentration is correspondingly diminishing.

Here, the initial steps of the decomposition pathways are considered. The first chemical event in the simulation is the breaking of the N-NO_2 bond and the dissociation of NO_2 fragments. At 200 fs of simulation time, the number of NO_2 fragments is 10, out of a possible total of 24, with some being successive elimination from the same HMX molecule. This preference to bond rupture is consistent with the recent observation that the energetic barriers for the cleavage of N-NO_2 bond in the solid phase of the nitramine RDX vary depending on the location of the molecule in the crystal. [73] At this stage of the simulation, the C-N bond breaking is also exhibited, occurring in two ways: the first (1) producing methylenenitramine ($CH_2N_2O_2$), while the symmetric breaking (2) leads to the formation of two $C_2H_4N_4O_4$ moieties, as shown below.

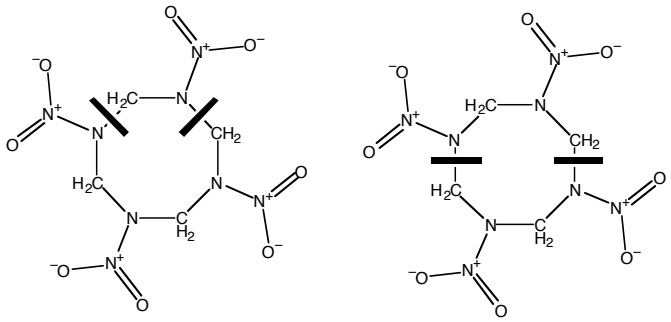

(1) (2)

Seven $CH_2N_2O_2$ species have been formed at around 200 fs of simulation time. These results are similar to those identified in thermal decomposition experiments. [58,62] A further N-NO_2 bond breaking then follows the decomposition (1) and (2) above. From (1), this leads to the formation of CH_2N and NO_2. These pathways are remarkably similar to those predicted previously by Melius from the decomposition of nitramines at fast

heating rates. [66]

As the radical CH_2N is formed, the production of HCN occurs via the reaction:

$$CH_2N + CH_2N \rightarrow C_2H_4N_2 \rightarrow HCN + CH_2NH.$$

Another source for the formation of HCN follows from a series of complex reactions that also produce nitric acid, HNO_3:

$$CH_2NH + NO_2 \rightarrow CH_3N_2O_2$$

$$CH_3N_2O_2 + NO_2 \rightarrow CH_2N_2O_3 + HNO$$

$$CH_2N_2O_3 \rightarrow HCN + HNO_3.$$

The schematic mechanism for these reactions is illustrated in Fig.4. It should be noted that formaldehyde, CH_2O, is first formed from a reaction involving large intermediate fragments. The formation occurs from the reaction of the $C_2H_4N_4O_4$ moiety, which is produced from the symmetric bond scission of the HMX molecule as in (2) above, with HNO. The reaction leads to the production of CH_2O and a larger intermediate fragment that undergoes further decomposition.

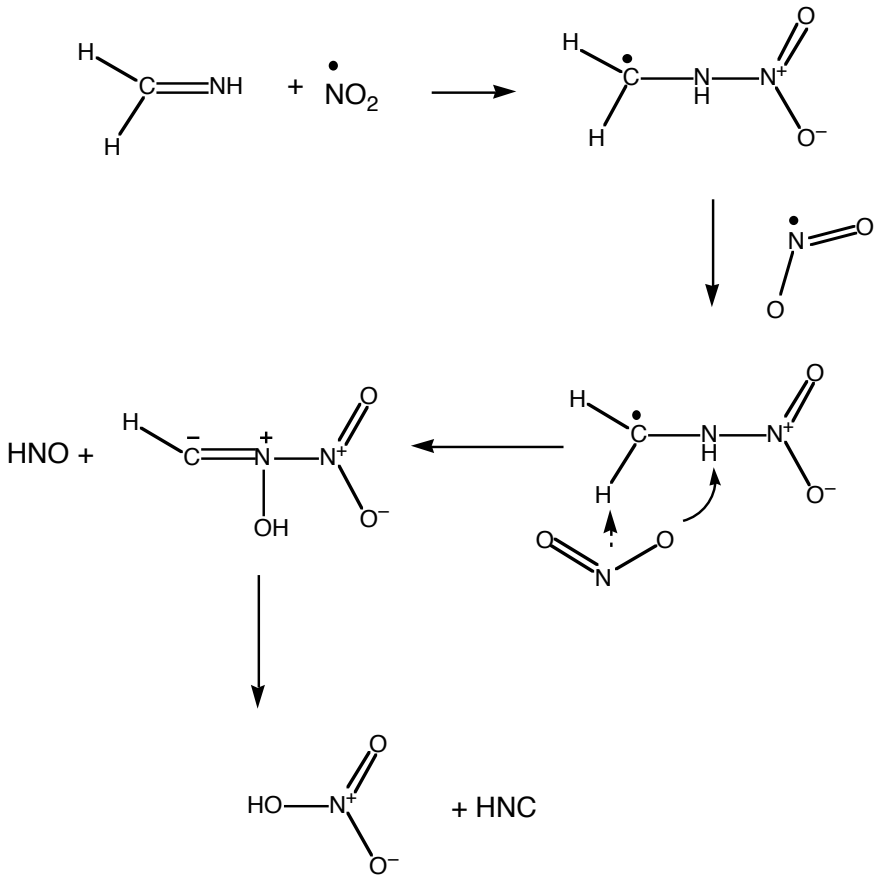

Figure 8. Reaction scheme for the formation of HCN.

CHEMISTRY OF TATB

It has been noted that explosives rich in carbon tend to have much longer reaction zones than those that do not. Such explosives form graphitic or diamond-like carbon particles during detonation. [74,75] Formation of the bulk solid carbon from the clusters is believed to play a key role in determining the size of the reaction zone of a given explosive. [75,76] The latter process is thought to be initiated by collecting carbon atoms from a relatively large volume and governed by diffusion-limited growth of these

clusters. TATB ($C_6H_6N_6O_6$, Figure 9) is an insensitive explosive with an estimated reaction zone in the microsecond regime. It's been found to be remarkably stable under extreme pressure, persisting metallization or chemical decomposition. [77,78] It can be described as markedly under oxidized, or alternatively, carbon rich. As a consequence, significant carbon formation in some form (graphite, clusters, or diamond) is expected to be part of its final products under detonation reactions.

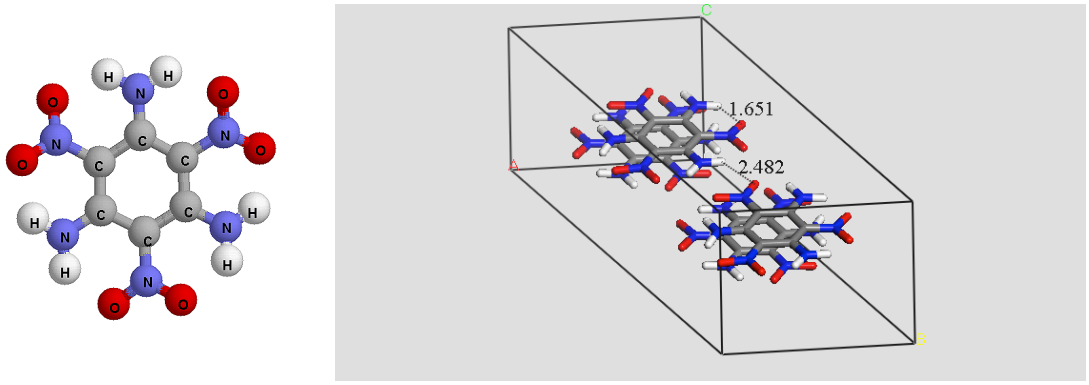

(a) (b)

Figure 10: (a) Molecular TATB ($C_6H_6N_6O_6$). (b) Graphite-like sheets in a 1x2x2 supercell of non-orthorhombic crystals of TATB solid phase. The x-ray crystal structure of TATB includes 2 molecules per unit cell (triclinic) with parameters a = 9.010, b = 9.028, c = 6.812 Å, and α = 108.59°, β = 91.82°, and γ = 119.97°. [79]

We used DFTB molecular dynamics to model the reactivity of TATB under thermal and shock conditions. Relatively few studies have been performed on the chemistry of stronger shocks due to the requirement for accurate methods of simulating a

variety of chemical reactions. In addition, our simulations have revealed an important feature of TATB decomposition: the first evidence for the formation of an extended region of nitrogen-rich heterocyclic clusters, the formation of which inhibits reactivity towards final decomposition products of fluid N_2 and solid carbon. [36] This result suggests a new mechanism for carbon-rich explosive materials that precedes the slow diffusion-limited process of forming the bulk solid from carbon clusters. Another important feature undisclosed previously in the reactivity of energetic materials at extreme conditions is the prevailing persistence of small charged species through out thermal and shock simulations.

Our thermal decomposition simulations were conducted at constant volume and temperature. Periodic boundary conditions were imposed in all directions, while constant temperature conditions were implemented through simple velocity rescaling. The probability to rescale atom velocities was chosen to be 0.1 per time step. A dynamic time-step of 0.48 fs was used. Several simulations with various density, size, and temperature were carried out: (1) four simulations used a 1X1X3 supercell (144 atoms) at density ρ= 2.87 g/cm^3, corresponding to an initial pressure of 29.7 GPa was thermally heated at various temperatures of T= 3500, 3000, 2500, and 1500° K, and (2) two simulations used a 2x2x1 supercell (192 atoms) at two densities ρ= 2.72 and ρ= 2.9 g/cm^3, corresponding to initial pressures of about 22 and 34.5 GPa, respectively, were thermally heated at T= 3000° K. These simulations varied in duration from 400 ps to 2.0 ns.

We also simulated crystal TATB's reactivity under steady overdriven shock compression using the MSST.[80,81] We performed MD simulations with a time step of 0.5

fs for up to 430 ps with shock speeds of 8 and 9 km/s, and 202 ps for a shock speed of 10 km/s on the smaller 1x1x2 computational cell. For the larger 1x2x2 supercell, the simulation was conducted up to 140 ps. In all simulations, initial position of TATB molecules were taken from the experimental x-ray structure, and then optimized with the DFTB method. Initial velocities were randomly chosen, with an initial temperature of 300° K. We then performed an equilibration for a period of up to 2 ps at temperature of 300° K. Shock compression occurred along the *c* lattice direction in all simulations.

In our shock simulations, TATB must be substantially overdriven to observe chemistry on sub-ns timescales**.** The experimental TATB detonation velocity is 7.7 km/s at ρ=1.88 g/cm^3 and a pressure of 29 GPa. Figure 10 displays the time evolution of the average temperature, stress, and volume for all three initial shock speeds. For the 9 km/s shock speed simulation, the temperature gradually increases from around 1900 to 3500° K, while the stress increases from 58 to 70 GPa. This is due to exothermic chemical reactions. More dramatic conditions are noted for the 10 km/s shock speed simulation, where the temperature increases from 2500° K to 3500° K and the stress reaches 85 GPa in less than 50 ps of simulation time. For the 8 km/s simulation, the temperature and stress have nearly constant values of 1500° K and 42 GPa throughout the simulation period. The only observed reactivity at this shock speed is protons transfer between amino and nitro groups up to 0.43 ns of simulation time. A similar observation is obtained from thermal heating at T=1500° K up to 2 ns. These results clearly indicate that chemical transformations occur faster as the temperature increases (or shock speed increases).

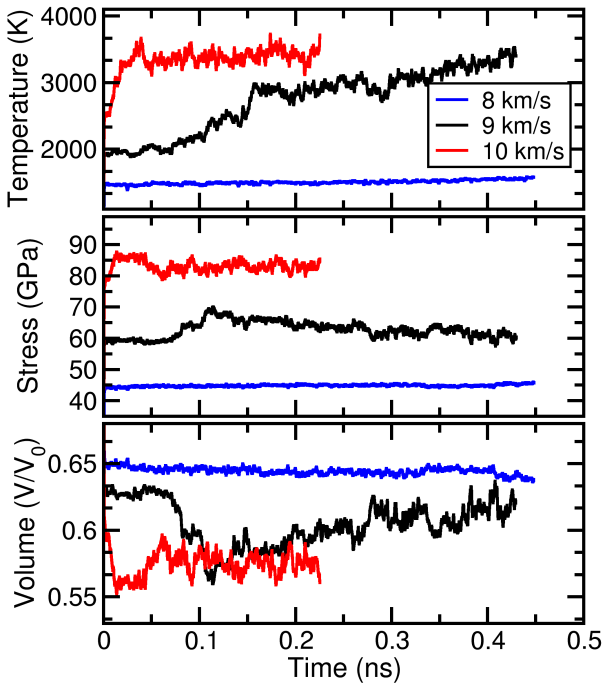

Figure 10. Time evolution of average temperature, shock-propagation-direction stress, and volume of 1x1x2 computational cell for simulations at shock speeds of 8, 9, and 10 km/s.

The use of quantum based methods permit us for the first time to examine electronic properties at detonation conditions. Our simulations of shocked nitromethane showed that a transient band-gap reduction to a semi-metallic state occurred during shock compression with a speed of 6.5 km/s.[35] Our shock simulations of TATB also show a non-monotonic change in electronic properties. Figure 11 compares the dimensionless electronic state overlap parameter, which is often used to characterize metallization,[82] of TATB and detonating nitromethane. With an overdriven shock speed of 9km/s, TATB is in a metallic state throughout most of the simulation. For a shock speed of 8 km/s, it stays mostly as an insulator, which is consistent with its lack of reactivity.

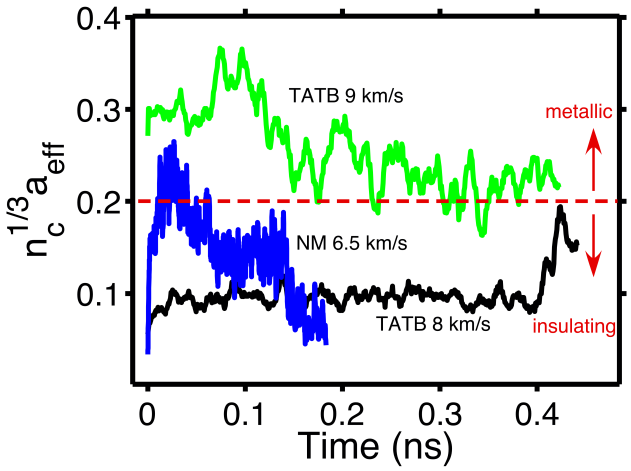

Figure 11. Time profile of the electronic state overlap parameter $n_c^{1/3}a_{eff}$ for TATB and nitromethane. n_c is the charge-carrier concentration, and a_{eff} is the effective Bohr radius of electronic states.

Global features of TATB decomposition obtained from both thermal and shock simulations revealed similar trends. The shock simulation with a speed of 9 km/s has a temperature range of about 1900-3500° K, allowing for comparison with thermal decomposition simulations within T=2500-3500° K. Both simulations types have fast chemical transformations, particularly at high T (e.g. T=3500° K). At this temperature, H_2O and N_2 dominant gas formation occurred in less than 100 ps, with water being first to appear. At the high T condition, dissociation-recombination reactions of the type $H_2O \leftrightarrow H + OH$ are very prevalent. Furazan-like structures seem to accompany H_2O formation. Once hydrogen is eliminated from amine groups to form water, nitrogen of adjacent molecules joins in to form N_2.

Unlike water, however, the formation of N_2 does not proceed before a polymerization process is underway in which the heavy fragments of the parent TATB have bonded together, as illustrated in Figure 12. Nitrogen formation can thus be described as having several growth steps: (1) elimination of H_2O and NO with furazan-like structures as intermediates, (2) formation of extended ring network (condensation reactions), and (3) later steps are always preceded by ring formation with N-N or N-N-N. It should be noted that experimental evidence for benzofurazan formation have been reported for decomposing TATB subjected to various stimuli such as heat, impact, or UV photolysis. [83]

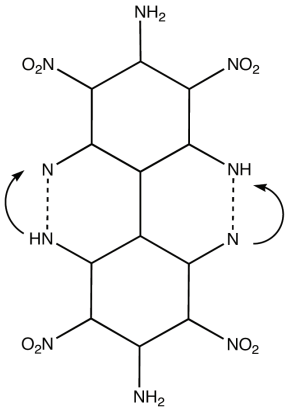

Figure 12. Condensation reactions (e.g. bimolecular) to form N-N bonds from parent fragments.

Fast chemistry in our thermal and shock simulations is also exhibited by the fact that both H_2O and N_2 appear to reach steady state of concentration at about 100 ps and 250 ps, respectively. Figure 13 displays the concentration profile of TATB and most dominant, stable products from the shock simulation with a speed of 9 km/s. Figure 14

shows the concentration profile of water from thermal decomposition simulations of two temperatures, T= 2500, and 3500° K at ρ= 2.87 g/cm^3, along with an exponential fit to obtain reaction rates of this product.

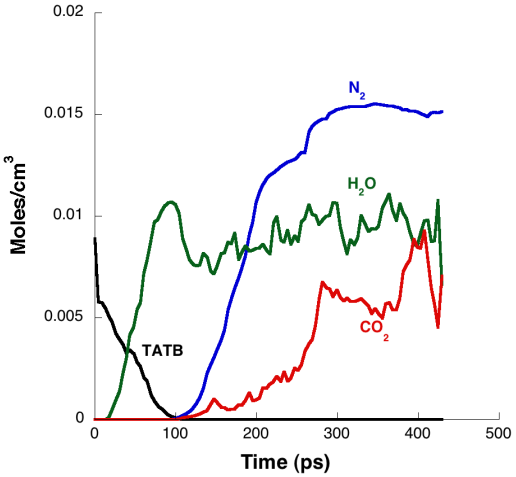

Figure 13. Concentration time profile of TATB and dominant gas products N_2, H_2O and CO_2, from the simulation with shock speed of 9 km/s.

We found that concentration profiles of stable products such as H_2O and N_2 can be fit to an expression of the form: $C(t) = C_\infty (1- e^{-bt})$, where C_∞ is the equilibrium concentration and b is the effective rate constant. From this fit to the data in Figure 14, we estimate effective reaction rates for the formation of H_2O to be 0.04 and 0.44 ps^{-1} for T=2500 and 3500° K, respectively. The shock simulation with a speed of 9 km/s also provides a similar fit for H_2O, and an effective rate of.02 ps^{-1}. A similar fit for N_2, as shown in Figure 15, at T=3500° yielded an effective rate of 0.11 ps^{-1}. The figure presents the N_2 concentration profile from thermal simulations at T=2500 and 3500° K, and from the shock simulation (insert). We note the similarities in N_2 delayed formation at

T=2500° and the shock simulation, along with its step-type formation due to "condensation reactions" of the type shown in Figure 12 above.

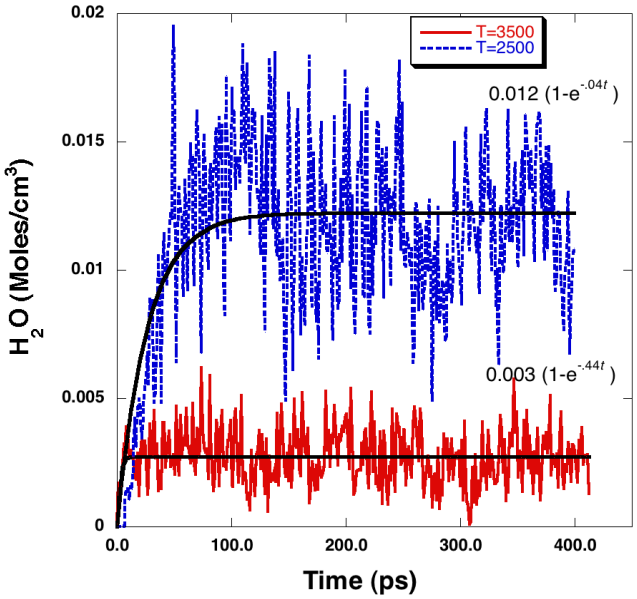

Figure 14. Water concentration profile from thermal decomposition simulations at T=2500 and 3500° K.

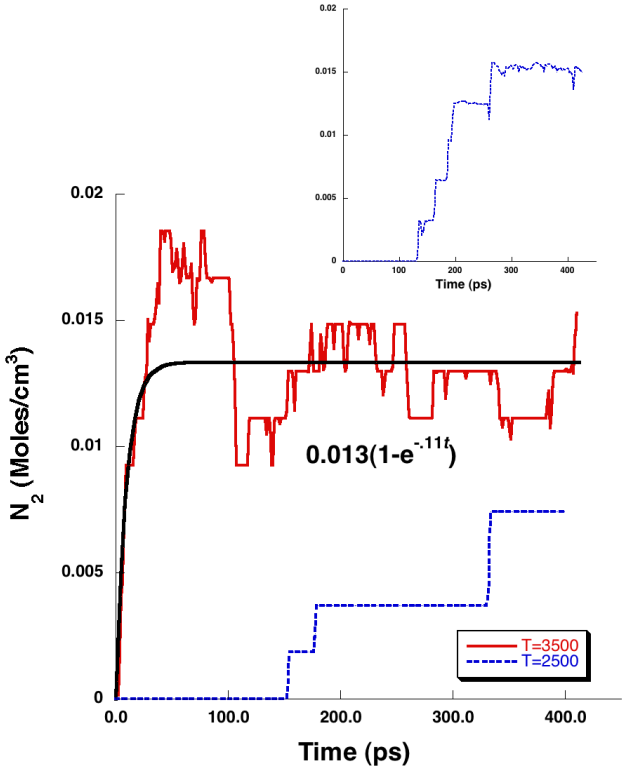

Figure 15. N_2 concentration profile from thermal decomposition simulations at T=2500 and 3500° K at ρ= 2.87 g/cm^3, and shock simulation with speed of 9 km/s (insert).

Our thermal and shock simulations revealed a very important step in TATB decomposition process: the formation of carbon-rich, nitrogen-rich heterocyclic clusters of various sizes. In Figure 16, we compare the results obtained from simulations of cell sizes of 1x1x2 and 1x2x2 for the shock simulation with a speed of 10 km/s. The plot shows the time profile of the average nitrogen to carbon ratio in carbon-containing clusters. As shown, both simulations confirm the formation of nitrogen-rich heterocycles, albeit at different time due to increased reactivity with increase in the shock speed. Figure

16 also shows the nitrogen contents variation in these clusters, ranging between 50% N and 100% N in the smaller cell simulation, and between 63 % N and 96% N in the larger1x2x2 simulation cell. In all of our thermal simulations we found that the formation of these heterocycles is persistent so much that no further decomposition occurred, even at the highest temperature. For example, the formation of high N clusters persists from ~50 ps to 0.42 ns at T=3500° K. This is a testament to the stability these clusters with respect to further decomposition and further slowing of the chemical reactivity of TATB. A representative heterocycle is shown in Figure 17.

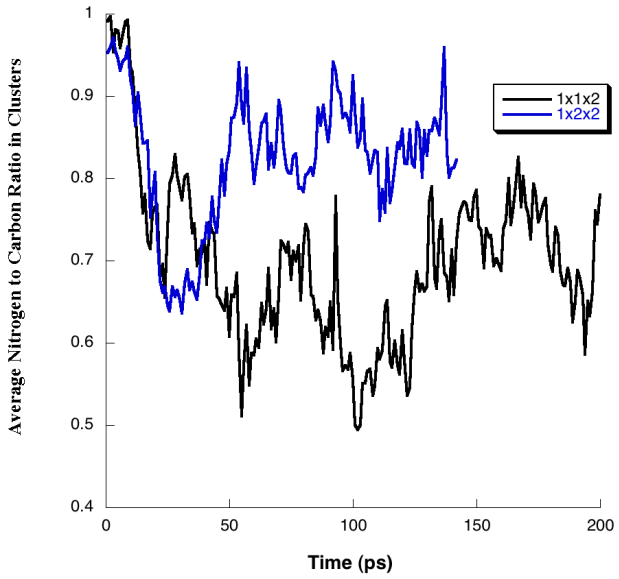

Figure 16. Time evolution of the average nitrogen to carbon ratio in carbon-containing clusters obtained from simulated shocked TATB experiencing a shock wave speed of 10 km/s.

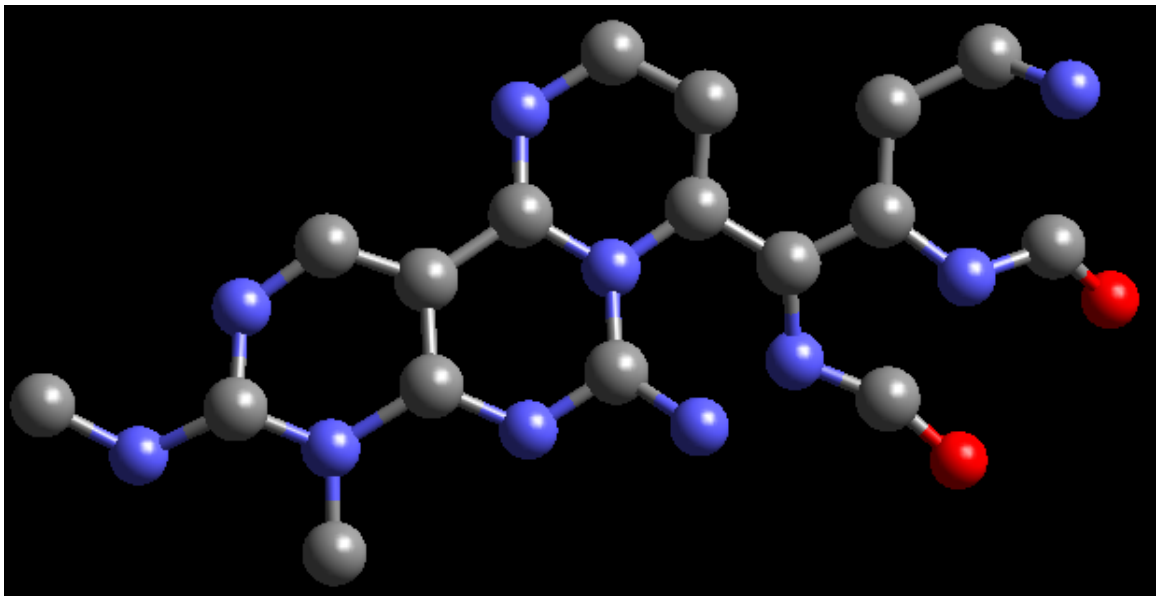

Figure 17: A representative nitrogen-rich heterocycle near the end of simulated TATB experiencing a steady shock wave with a speed of 9 km/s.

Finally, our MD simulations are providing very detailed decomposition mechanism for TATB[84]. We have been able to construct a preliminary four-step decomposition mechanism for use in hydrodynamic grain scale simulations (e.g. micron–size pore collapse in TATB). The first step involves the decomposition of TATB into mono-furazan and water, followed by the formation of di-furazan and water. The third step accounts for the formation of high-nitrogen heterocycles and other gaseous products such as water, N_2, and CO from condensation reactions. The last step involves further decomposition of these heterocycles into N_2 and the final formation of graphite. We obtained Arrhenius parameters for the expression $K=Ae^{-Ea/RT}$, with A being the prefactor and Ea is the activation energy, for each mechanistic step from fit of rates at different temperatures. These parameters are shown in Table I for the five steps mechanism. Using these kinetics parameters in the thermochemical equilibrium code Cheetah

provided good agreement with our MD-based decomposition kinetics at these various T, with an example shown in Figure 16. Refinement of this overall decomposition mechanism to a desired accuracy is always possible through inclusion of more detailed steps from our atomistic simulations.

Table I. Arrhenius parameters for a reduced four-steps decomposition mechanism of TATB.

Mechanistic Step	Prefactor (in μs^{-1})	Activation Energy (in °K)
TATB → Mono-furazan + H_2O	$2.0X10^6$	$3.1X10^4$
Mono-furazan → Di-furazan + H_2O	$3.2X10^3$	$1.74X10^4$
2 (Di-furazan) → $4N_2 + 2H_2O + 6CO + 2C_3N_2$	$0.75X10^6$	$3.0X10^4$
C_3N_2 → Graphite + N_2	$2.0X10^7$	$4.0X10^4$

CONCLUSIONS

Our thermal and shock simulations allow us to (a) incorporate high-pressure reaction rates in thermochemical-hydro-codes to simulate high explosive reactivity under various scenarios, including grain-scale dynamics, (b) enhance thermo-chemical modeling capabilities by providing a complete account of relevant species, and (c) obtain a "reduced" reaction sets from insight into detailed decomposition pathways.

Our results are useful in determining the nature of the Chapman-Jouguet detonation state.[45] Thermodynamic models of detonation have long assumed that the Chapman-Jouguet state was composed primarily of small gas species and condensed solid particles[85]. Our studies on oxygen-rich explosives, such as PETN[50], HMX[34], and NM[19] confirm this picture, with the strong caveat that hydrogen becomes highly diffusive and non-molecular. We find that the more sensitive, high-performing HMX explosive produces mostly small gas species such as water and N_2. In contrast, the low-performing, insensitive TATB explosive produces large, stable, high-nitrogen, carbon-rich heterocycles, which retard TATB's complete reactivity towards a final form of carbon (graphite or diamond). Our results on TATB indicate that the inclusion of nanoparticles in thermodynamic models[86] could be required to accurately describe speciation at extreme conditions.

The methods used to study the complex chemistry under extreme conditions are also applicable to other instances where organic materials are subjected to strong shock waves. A good example of this is the impact of comets upon the earth and the possible formation of precursor molecules to life.[87] We believe that knowledge of the chemistry of shocked organic matter will continue to develop rapidly as new computational and experimental[88] tools become available.

ACKNOWLEDGEMENTS

The authors thank Nir Goldman, I-F Will Kuo, Amitesh Maiti, Evan J. Reed, and Christine J. Wu for many invaluable contributions to the work discussed in this review. We particularly remember the many insights and contributions of our recently deceased colleague, W. Michael Howard. This research was performed under the auspices of the

U.S. Department of Energy by Lawrence Livermore National Laboratory under Contract No. DE-AC52-07NA27344.

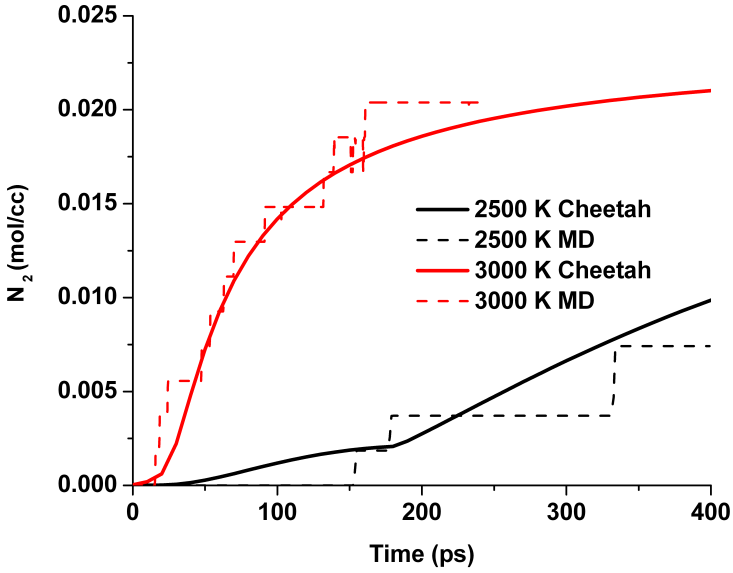

Figure 18: A comparison between the thermochemical prediction of the formation of N_2 based on the four-steps reduced TATB decomposition mechanism, and DFTB-MD thermal decomposition calculations at T= 2500 and 3000 °K.

References:

(1) Campbell, A. W.; Davis, W. C.; Ramsay, J. B.; Travis, J. R. Detonation and chemistry. *Phys. Fluids* **1961**, *4*, 511.

(2) Dremin, A. N.; Savrov, S. D.; Trofimov, V. S.; Shvedov, K. K.: *Detonation Waves in Condensed Matter*; Nauka: Moscow, 1970.

(3) Elban, W. L.; Armstrong, R. W.; Yoo, K. C.; Rosemeier, R. G.; Yee, R. Y. Det. Chemistry. *J. Mater.Sci* **1989**, *24*, 1273.

(4) Enikolopyan, N. S. Det and Chemistry. *Dokl. Akad. Nauk SSSR* **1985**, *283*, 612.

(5) Kanel, G. I.; Razorenov, S. V.; Utkin, A. V.; Fortov, V. E.: *Impact-Wave Phenomena in Condensed Matter*; Yanus-K: Moscow, 1996.

(6) Miles, M. H.; Dickinson, J. T. Det and chem. *Appl. Phys. Lett.* **1982**, *41*, 924.

(7) Tarver, C. M.; Chidester, S. K.; Nichols III, A. L. critical conditions for impact and shockhot spot in solid explosives. *J. Phys. Chem.* **1996**, *100*, 5794.

(8) Bowden, F. P.; Yoffe, A. D.: *Initiation and Growth of Explosion in Liquids and Solids*; Cambridge University Press: London, 1952.

(9) Coffey, C. S. islocation initiation. *Phys. Rev. B* **1981**, *24*, 6984.

(10) Hawthorne, S. B.; Lagadec, A. J. M.; Kalderis, D.; Like, A. V.; Miller, D. J. HE Hazard. *Environ. Sci. Technol.* **2000**, *34*, 3224.

(11) Fried, L. E.; Manaa, M. R.; Pagoria, P. F.; Simpson, R. L. Design and Synthesis of Energetic Materials. *Annu. Rev. Mater. Res.* **2001**, *31*, 291.

(12) Sorescu, D. C.; Rice, B. M. Theoretical Predictions of Energetic Molecular Crystals at Ambient and Hydrostatic Compression Using Dispersion Corrections to DFT (DFT-D). *J. Phys. Chem. C* **2010**, *114*, 6734-6748.

(13) Elstner, M.; Porezag, D.; Jungnickel, G.; Elsner, J.; Hauk, M.; Frauenheim, T.; Suhai, S.; Seifert, G. DFTB. *Phys. Rev. B* **1998**, *58*, 7260.

(14) Hemley, R. J. The effect of high pressure on molecules. *Ann. Rev. Phys. Chem.* **2000**, *51*, 763-800.

(15) Kohn, W.; Sham, L. J. DFT. *Phys. Rev.* **1965**, *140*, A1133.

(16) Ancilotto, F.; Chiarotti, G. L.; Scandolo, S.; Tosatti, E. Dissociation of methane at extreme pressure and temperature. *Science* **1997**, *275*, 1288.

(17) Cavazzoni, C.; Chiarotti, G. L.; Scandolo, S.; Tosatti, E.; Bernasconi, M.; Parrinello, M. ab initio/MD of H2O and NH3 at extreme conditions. *Science* **1999**, *283*, 44.

(18) Goldman, N.; Reed, E. J.; Fried, L. E.; Kuo, I. F. W.; Maiti, A. Synthesis of glycine-containing complexes in impacts of comets on early Earth. *Nature Chemistry* **2010**, *2*, 949-954.

(19) Manaa, M. R.; Reed, E. J.; Fried, L. E.; Galli, G.; Gygi, F. Early Chemistry in hot dense nitromethane. *J. Chem. Phys.* **2004**, *120*, 10146.

(20) Mundy, C. J.; Curioni, A.; Goldman, N.; Kuo, I. F. W.; Reed, E. J.; Fried, L. E.; Ianuzzi, M. Ultrafast transformation of graphite to diamond: An ab initio study of graphite under shock compression. *Journal of Chemical Physics* **2008**, *128*.

(21) van Duin, A. C. T.; Dasgupta, S.; Lorant, F.; Goddard III, W. A. REAXFF. *J. Phys. Chem. A* **2001**, *105*, 9396.

(22) Budzien, J.; Thompson, A. P.; Zybin, S. V. Reactive Molecular Dynamics Simulations of Shock Through a Single Crystal of Pentaerythritol Tetranitrate. *Journal of Physical Chemistry B* **2009**, *113*, 13142-13151.

(23) Han, S. P.; van Duin, A. C. T.; Goddard, W. A.; Strachan, A. Thermal Decomposition of Condensed-Phase Nitromethane from Molecular Dynamics from ReaxFF Reactive Dynamics. *Journal of Physical Chemistry B* **2011**, *115*, 6534-6540.

(24) Strachan, A.; Kober, E. M.; van Duin, A. C. T.; Oxgaard, J.; Goddard, W. A. Thermal decomposition of RDX from reactive molecular dynamics. *Journal of Chemical Physics* **2005**, *122*.

(25) Strachan, A.; van Duin, A. C. T.; Chakraborty, D.; Dasgupta, S.; Goddard, W. A. Shock waves in high-enegy materials (RDX). *Phys. Rev. Lett.* **2003**, *91*, 098301.

(26) Zhang, L. Z.; van Duin, A. C. T.; Zybin, S. V.; Goddard, W. A. Thermal Decomposition of Hydrazines from Reactive Dynamics Using the ReaxFF Reactive Force Field. *Journal of Physical Chemistry B* **2009**, *113*, 10770-10778.

(27) Zhou, T. T.; Zybin, S. V.; Liu, Y.; Huang, F. L.; Goddard, W. A. Anisotropic shock sensitivity for beta-octahydro-1,3,5,7-tetranitro-1,3,5,7-tetrazocine energetic material under compressive-shear loading from ReaxFF-lg reactive dynamics simulations. *Journal of Applied Physics* **2012**, *111*.

(28) Zybin, S. V.; Goddard, W. A.; Xu, P.; van Duin, A. C. T.; Thompson, A. P. Physical mechanism of anisotropic sensitivity in pentaerythritol tetranitrate from compressive-shear reaction dynamics simulations. *Applied Physics Letters* **2010**, *96*.

(29) Aktulga, H., M.; Fogarty, J. C.; Pandit, S. A.; Grama, A. Y. Parallel reactive molecular dynamics: Numerical methods and algorithmic techniques. *Parallel Computing* **2012**, *38*, 245-259.

(30) Bickham, S. R.; Kress, J. D.; Collins, L. A. Molecular dynamics simulations of shocked benzene. *J. Chem. Phys.* **2000**, *112*, 9695.

(31) Kress, J. D.; Bickham, S. R.; Collins, L. A.; Holian, B. L.; Goedecker, S. Tight-binding molecular dynamics of hock waves in methane. *Phys. Rev. Lett.* **1999**, *83*, 3896.

(32) Qi, T. T.; Reed, E. J. Simulations of Shocked Methane Including Self-Consistent Semiclassical Quantum Nuclear Effects. *Journal of Physical Chemistry A* **2012**, *116*, 10451-10459.

(33) Ge, N. N.; Wei, Y. K.; Ji, G. F.; Chen, X. R.; Zhao, F.; Wei, D. Q. Initial Decomposition of the Condensed-Phase beta-HMX under Shock Waves: Molecular Dynamics Simulations. *Journal of Physical Chemistry B* **2012**, *116*, 13696-13704.

(34) Manaa, M. R.; Fried, L. E.; Melius, C. F.; Elstner, M.; Frauenheim, T. Decomposition of HMX at extreme conditions:MD. *J. Phys. Chem. A* **2002**, *106*, 9024.

(35) Reed, E. J.; Manaa, M. R.; Fried, L. E.; Glaesemann, K. R.; Joannopoulos, J. D. A transient semimetallic layer in detonating nitromethane. *Nature Physics* **2008**, *4*, 72-76.

(36) Manaa, M. R.; Reed, E. J.; Fried, L. E.; Goldman, N. Nitrogen-Rich Heterocycles as Reactivity Retardants in Shocked Insensitive Explosives. *Journal of the American Chemical Society* **2009**, *131*, 5483-5487.

(37) Reed, E. J.; Rodriguez, A. W.; Manaa, M. R.; Fried, L. E.; Tarver, C. M. Ultrafast Detonation of Hydrazoic Acid (HN3). *Physical Review Letters* **2012**, *109*.

(38) Margetis, D.; Kaxiras, E.; Elstner, M.; Frauenheim, T.; Manaa, M. R. Electronic structure of solid nitromethane:high-pressure. *J. Chem. Phys.* **2002**, *117*, 788.

(39) Perdew, J. P.; Burke, K.; Ernzerhof, M. PBE. *Phys. Rev. Lett.* **1997**, *78*, 1396.

(40) Yang, Y.; Yu, H.; York, D.; Cui, Q.; Elstner, M. Extension of the Self-Consistent-Charge Density-Functional Tight-Binding Method: Third-Order Expansion of the Density Functional Theory Total Energy and Introduction of a Modified Effective Coulomb Interaction. *J. Phys. Chem. A* **2007**, *111*, 10861-10873.

(41) Goldman, N.; Fried, L. E. Extending the Density Functional Tight Binding Method to Carbon Under Extreme Conditions. *J. Phys. Chem. C* **2011**, *116*, 2198-2204.

(42) Goldman, N.; Goverapet Srinivasan, S.; Hamel, S.; Fried, L. E.; Gaus, M.; Elstner, M. Determination of a Density Functional Tight Binding Model with an Extended Basis Set and Three-Body Repulsion for Carbon Under Extreme Pressures and Temperatures. *J. Phys. Chem. C* **2013**, *117*, 7885-7894.

(43) Holian, B. L. NEMD of shock induced placticity. *Phys. Rev. A* **1988**, *37*, 2562.

(44) Reed, E. J.; Fried, L. E.; Joannopoulos, J. D. A method for Tractable Dynamical Studies of shock compression. *Phys. Rev. Lett.* **2003**, *90*, 235503.

(45) Fickett, W.; Davis, W. C.: *Detonation*; University of California Press: Berkeley, 1979.

(46) Maillet, J. B.; Mareschal, M.; Soulard, L.; Ravelo, R.; Lomdahl, P. S.; Germann, T. C.; Holian, B. L. *Phys. Rev. E* **2001**, *63*, 016121.

(47) Reed, E. J. Electron-Ion Coupling in Shocked Energetic Materials. *J. Phys. Chem. C* **2012**, *116*, 2205-2211.

(48) Maillet, J. B.; Bourasseau, E. Ab initio simulations of thermodynamic and chemical properties of detonation product mixtures. *J. Chem. Phys.* **2009**, *131*, 084107.

(49) Goldman, N.; Reed, E. J.; Fried, L. E. Quantum mechanical corrections to simulated shock Hugoniot temperatures. *J. Chem. Phys.* **2009**, *131*, 204103.

(50) Wu, C. J.; Fried, L. E.; Yang, L. H.; Goldman, N.; Bastea, S. Catalytic behavior of dense hot water. *Nature Chemistry* **2009**, *1*, 57-62.

(51) Goldman, N.; Fried, L. E.; Kuo, I. F. W.; Mundy, C. J. Bonding in the superionic phase of water. *Phys. Rev. Lett.* **2005**, *94*, 217801.

(52) Behrens, R. Decomposition of HMX. *Int. J. Chem. Kinet.* **1990**, *22*, 135.

(53) Behrens, R. Decomposition of HMX. *J. Phys. Chem.* **1990**, *94*, 6706.

(54) Behrens, R.; Bulusu, S. HMX decomposition. *J. Phys. Chem.* **1991**, *95*, 5838.

(55) Brill, T. B. Combustion of HMX. *J. Prop. Power* **1995**, *11*, 740.

(56) Brill, T. B.; Gongwer, P. E.; Williams, G. K. decomp HMX. *J. Phys. Chem.* **1994**, *98*, 12242.

(57) Bulusu, S.; Axenrod, T.; Milne, G. W. A. HMX decomposition. *Org. Mass. Spectrom.* **1970**, *3*, 13.

(58) Farber, M.; Srivastava, R. D. In *Tilte*1979; CPIA pub.

(59) Fifer, R. A.: Fundamentals of Solid Propellant Combustion. In *Progress in Astronautics and Aeronautics*; Kuo, K. K., Summerfield, M., Eds.; AIAA Inc.: New York, 1984; Vol. 90; pp 177.

(60) Morgan, C. V.; Bayer, R. A. HMX thermal decomposition. *Combust. Flame* **1979**, *36*, 99.

(61) Oxley, J. C.; Kooh, A. B.; Szekers, R.; Zhang, W. HMX decomposition. *J. Phys. Chem.* **1994**, *98*, 7004.

(62) Suryanarayana, B.; Graybush, R. J.; Autera, J. R. HMX1. *Chem. Ind. London* **1967**, *52*, 2177.

(63) Tang, C.-J.; Lee, Y. J.; Kudva, G.; Litzinger, T. A. Combustion of HMX. *Combust. Flame* **1999**, *117*, 170.

(64) Tang, C.-J.; Lee, Y. J.; Litzinger, T. A. combustion of HMX. *J. Prop. Power* **1999**, *15*, 296.

(65) Politzer, P.; Boyd, S. *Struct. Chem.* **2002**, *13*, 105.

(66) Melius, C. F.: HMX decomposition. In *Chemistry and Physics of Energetic Materials*; Bulusu, D. N., Ed.; Kluwer: Dordercht, 1990.

(67) Lewis, J. P.; Glaesemann, K. R.; Van Opdorp, K.; Voth, G. A. HMX. *J. Phys. Chem. A* **2000**, *104*, 11384.

(68) Chakraborty, D.; Muller, R. P.; Dasgupta, S.; Goddard III, W. A. unimolecular decomposiion of HMX. *J. Phys. Chem. A* **2001**, *105*, 1302.

(69) Zhang, L. Z.; Zybin, S. V.; van Duin, A. C. T.; Dasgupta, S.; Goddard, W. A.; Kober, E. M. Carbon Cluster Formation during Thermal Decomposition of Octahydro-1,3,5,7-tetranitro-1,3,5,7-tetrazocine and 1,3,5-Triamino-2,4,6-trinitrobenzene High Explosives from ReaxFF Reactive Molecular Dynamics Simulations. *Journal of Physical Chemistry A* **2009**, *113*, 10619-10640.

(70) Landers, A. G.; Brill, T. B. HMX phase-transition. *J. Phys. Chem.* **1980**, *84*, 3573.

(71) Fried, L. E.; Howard, W. M. cheetah. *J. Chem. Phys.* **1998**, *109*, 7338.

(72) Fried, L. E.; Howard, W. M. cheetah. *Phys. Rev. B* **2000**, *61*, 8734.

(73) Kuklja, M. M. dissociation near a void. *J. Phys. Chem. B* **2001**, *105*, 10159.

(74) Greiner, N. R.; Phillips, D. S.; Johnson, J. D.; Volk, F. DIAMONDS IN DETONATION SOOT. *Nature* **1988**, *333*, 440-442.

(75) Shaw, M. S.; Johnson, J. D. CARBON CLUSTERING IN DETONATIONS. *Journal of Applied Physics* **1987**, *62*, 2080-2085.

(76) Viecelli, J. A.; Ree, F. H. Carbon clustering kinetics in detonation wave propagation. *Journal of Applied Physics* **1999**, *86*, 237-248.

(77) Davidson, A. J.; Dias, R. P.; Dattelbaum, D. M.; Yoo, C. S. "Stubborn" triaminotrinitrobenzene: Unusually high chemical stability of a molecular solid to 150 GPa. *Journal of Chemical Physics* **2011**, *135*.

(78) Manaa, M. R.; Fried, L. E. Nearly Equivalent Inter- and Intramolecular Hydrogen Bonding in 1,3,5-Triamino-2,4,6-trinitrobenzene at High Pressure. *Journal of Physical Chemistry C* **2012**, *116*, 2116-2122.

(79) Cady, H. H.; Larson, A. C. crystal structure of TATB. *Acta Crystallogr.* **1965**, *18*, 485.

(80) Reed, E. J.; Fried, L. E.; Joannopoulos, J. D. A method for tractable dynamical studies of single shock compression. *Phys. Rev. Lett.* **2003**, *90*, 2355031.

(81) Reed, E. J.; Fried, L. E.; Manaa, M. R.; Joannopoulos, J. D.: A multi-scale approach to molecular dynamics simulations of shock waves. In *Chemistry at Extreme Conditions*; Manaa, M. R., Ed.; Elsevier B. V.: Amsterdam,, 2005; pp 297-326.

(82) Mott, N. F.: *Metal-Insulator Transitions*; Taylor and Francis: Bristol, 1990.

(83) Sharma, J.; Forbes, J. W.; Coffey, C. S.; Liddiard, T. P. The physical and chemical nature of sensitization centersz left from ot spots caused in triaminotrinitrobenzene by shock or impact. *J. Phys. Chem.* **1987**, *91*, 5139-5144.

(84) Fried, L. E.; Najjar, F.; Howard, W. M.; Manaa, M. R.; Reed, E. J.; Goldman, N.; Bastea, S.; Nichols, A. L. I. In *Tilte*, Couer d'Alene, Idaho, 2011, 2010; Pereis, S., Boswell, C., Asay, B.s; Office of Naval Research.

(85) Bastea, S.; Fried, L. E.: Chemical Equilibrium Detonation. In *Shock Wave Science and Technology Reference Library*; Zhang, F., Ed.; Springer-Verlag: Berlin Heidelberg, 2012; Vol. 6; pp 1-27.

(86) Bourasseau, E.; Maillet, J. B. Coupling microscopic and mesoscopic scales to simulate chemical equilibrium between a nanometric carbon cluster and detonation products fluid. *Phys. Chem. Chem. Phys.* **2011**, *13*, 7019-7039.

(87) Goldman, N.; Reed, E. J.; Fried, L. E.; Kuo, I. F. W.; Maiti, A. Synthesis of glycine-containing complexes in impacts of comets on early Earth. *Nature Chemistry* **2010**, *2*, 949-954.

(88) Dang, N. C.; Bolme, C. A.; Moore, D. S.; McGrane, S. D. Shock Induced Chemistry in Liquids Studied With Ultrafast Dynamic Ellipsometry and Visible Transient Absorption Spectroscopy. *J. Phys. Chem. A* **2012**, *116*, 10301-10309.